

Double white dwarf binary population in MOCCA star clusters

Comparisons with observations of close and wide binaries

L. Hellström¹, M. Giersz¹, A. Hypki^{1,3}, D. Belloni², A. Askar¹, G. Wiktorowicz¹

¹ Nicolaus Copernicus Astronomical Center, Polish Academy of Sciences, ul. Bartycka 18, PL-00-716 Warsaw, Poland
e-mail: hellstrom@camk.edu.pl

² Departamento de Física, Universidad Técnica Federico Santa María, Av. España 1680, Valparaíso, Chile

³ Faculty of Mathematics and Computer Science, A. Mickiewicz University, Uniwersytetu Poznańskiego 4, 61-614 Poznań, Poland

Accepted XXX. Received YYY; in original form ZZZ

ABSTRACT

There could be a significant population of double white dwarf binaries (DWDs) inside globular clusters (GCs), however, these are often too faint to be individually observed. We have utilized a large number GC models evolved with the Monte Carlo Cluster Simulator (MOCCA) code, to create a large statistical dataset of DWDs. These models include multiple-stellar populations, resulting in two distinct initial populations: one dense and another less dense. Due to the lower density of one population, a large number of objects escape during the early GC evolution, leading to a high mass-loss rate. In this dataset we have analysed three main groups of DWDs, namely in-cluster binaries, escaped binaries, and isolated evolution of primordial binaries. We compared the properties of these groups to observations of close and wide binaries. We find that the number of escaping DWDs is significantly larger than the number of in-cluster binaries and those that form via the isolated evolution of all primordial binaries in our GC models. This suggests that dynamics play an important role in the formation of DWDs. For close binaries, we found a good agreement in the separations of escaped binaries and isolated binaries, but in-cluster binaries showed slight differences. We could not reproduce the observed extremely low mass WDs due to the limitations of our stellar and binary evolution prescriptions. For wide binaries, we also found a good agreement in the separations and masses, after accounting for observational selection effects. We conclude that, even though the current observational samples of DWDs are extremely biased and incomplete, our results compare reasonably well with observations.

Key words. white dwarfs – globular clusters: general – binaries: general Methods: numerical – Methods: statistical

1. Introduction

Globular clusters (GCs) are self-gravitating spherical collections of tens of thousands to up to several millions of stars. The cores of these clusters are very dense (up to $\sim 10^6$ stars per pc^3), making stellar collisions and dynamical interactions relatively frequent. These interactions can affect not only the stars but also the cluster as a whole. For a binary, an interaction with another star can lead to a hardening or softening, depending on the interaction. It can also lead to the formation of a whole new binary through an exchange or a merger in a three-body or four-body interaction. In some cases, these interactions can even disrupt the binary so that it dissolves. During a three-body interaction, binaries can increase the kinetic energy of a third object or of the binary's centre of mass.

Globular clusters are generally very old and without any ongoing star formation. This causes them to almost exclusively contain old stars and, combined with the fact that they are found in almost all galaxies, makes them very interesting targets for observations and theoretical studies. Because of this, several research groups around the world are working on codes to simulate the evolution of these clusters, in order to better understand their evolution. Some examples of these codes include but are not limited to the *moCCA* code (Giersz et al. 2013), *cmc* (Kremer et al. 2020; Rodriguez et al. 2021), *nbody6++GPU* (Wang et al. 2015, 2016; Kamlah et al. 2022; Arca Sedda et al. 2024), *nbody7* (Banerjee 2022) and *PeTar* (Wang et al. 2020).

White dwarfs (WDs) are relatively abundant in GCs (Torres et al. 2015) and often make up a large portion of the stellar population. White dwarfs are important objects inside clusters since they can, among other things, be used to determine the age of their host cluster (e.g. Fontaine et al. 2001). The cooling process of WDs has been believed to be quite well understood so observations of their temperature and luminosity can be used to determine the age of the WD and thus the cluster. However, recent developments in understanding the physical processes occurring during their cooling have been challenging this picture (e.g. Bédard et al. 2024)

There are several different populations of WDs. The first and most basic one is that composed of single WDs. Another sizeable population is made up of detached binaries hosting main-sequence (MS) stars. In this case, the WD and the MS star have a wide enough orbit so that each star does not fill its Roche lobe and thus there is no ongoing mass transfer Campos et al. (2018). The semi-detached counterpart of these systems is called cataclysmic variable. A cataclysmic variable is a binary with a WD and a Roche-lobe filling secondary star, typically a MS star. These binaries are very tight with a short period ($\sim 1 - 6$ h) such that the secondary fills its Roche lobe and transfers mass onto the WD. This mass transfer typically results in an accretion disk around the WD which often can be seen in ultraviolet and X-ray observations. The last population of WDs we consider are the focus of this paper and corresponds to double WD binaries (DWDs) which consist of two WDs.

Double WD binaries can, in general, form in two ways: the progenitors to the WDs were formed together in a binary system (Belloni & Schreiber 2023a) or the binary was formed during a dynamical interaction (Kratter 2011). The resulting DWD can have different properties depending on the formation mechanism. Properties of primordial DWDs, that is, DWDs forming from the evolution of primordial binaries, depend on the initial binary parameter distribution of primordial binaries. The eccentricity distribution of a population of primordial binaries will have a thermal distribution while a population of dynamically formed binaries will have higher eccentricities than a thermal distribution. Meanwhile, the semi-major axis distribution of primordial binaries will depend on the initial distributions while for dynamically formed binaries it depends on the properties of the dense environment and gravitational encounters in which the binary is formed. In addition to this, due to the dense environments where DWDs are formed, it is likely that the binary can eventually experience more dynamical interactions which may affect the semi-major axis further.

Since DWDs can be observed across the electromagnetic spectrum and with planned gravitational wave detectors, they are known as multi-messenger sources. Both ground- and space-based telescopes and observatories can detect and measure WDs by electromagnetic radiation. Double WD binaries can emit radiation in a wide range of wavelengths, from optical to X-rays. In addition, with more precise and sensitive gravitational wave (GW) detectors, it will be possible to detect DWDs through the GW radiation they emit (Liu 2009; Maselli et al. 2020; Carvalho et al. 2022; Amaro-Seoane et al. 2023). Finally, there are speculations that neutrinos produced in the core of WDs can be detected and used as probes to study the interiors of the WDs (Drewes et al. 2022).

Recent studies have indicated that massive WDs most likely dominate the inner-most regions of core-collapsed GCs such as NGC 6397 (Kremer et al. 2021). These populations are, through dynamical interactions, stopping the cluster from completely collapsing. This produces very tight, inspiraling WD binaries that may be observed with future telescopes.

This paper will focus on DWDs from simulations of GCs with multiple-stellar populations (Lee et al. 1999; Gratton et al. 2012; Bastian & Lardo 2018). We will focus on in-cluster, escaped and isolated binaries (i.e. binaries with the same properties as the ones inside the clusters but evolved in isolation without dynamical interactions or relaxation affecting them). These binaries are then compared to observations of DWDs in two regions; close binaries where the data is retrieved from Brown et al. (2020), Kosakowski et al. (2023) and Schreiber et al. (2022) and wide binaries where the data is retrieved from El-Badry et al. (2021) and Heintz et al. (2022). This was done to get a better understanding of how realistic the DWD populations are in clusters from our simulations. We also wanted to find out if there are differences between the DWD populations inside and outside of clusters (escapers and binaries evolved in isolation). Finding any potential differences would be an important discovery since it could aid with determining the origin of observed WD binaries. This also relates to an upcoming study where we will investigate the GW signals from WD binaries, if we would find differences in these populations then we can also expect to see differences in their respective GW signals. This comparison, however, proved to be more difficult than we expected, due to severe limitations in the parameter space of observations, we have to limit our data greatly in order to make a proper comparison. Nevertheless, when restricting our data in ways that agree with observational

techniques and limitations we find good agreements everywhere except for the masses of close DWDs.

2. Observational sample

2.1. Close binaries

The data for close DWDs are obtained from Brown et al. (2020), Kosakowski et al. (2023) and Schreiber et al. (2022). Brown et al. (2020) uses the Extremely low mass (ELM) survey to find a sample of 98 detached, close double WD binaries. This survey targeted $< 0.3 M_{\odot}$ helium-core WDs binaries with periods between 0.0089 and 1.5 day. The absolute magnitude in the G band of the faintest object in this sample is 11.24 mag. These WDs are so close to each other that they cannot be resolved separately. Therefore this magnitude limit is for both WDs combined. Kosakowski et al. (2023) is a continuation of the ELM survey where they found 28 additional DWDs. Schreiber et al. (2022) collected 57 close DWDs from different surveys and did not limit themselves to ELMs.

2.2. Wide binaries

For wide binaries we use the published catalogue from Heintz et al. (2022) which contains data of 1590 wide DWDs from Gaia EDR3 (Gaia Collaboration et al. 2021) and El-Badry et al. (2021). The goal of Heintz et al. (2022) was to check existing methods for determining WD ages. They used wide DWDs, separated by more than 100 au, and made the assumption that at these distances, the stars would evolve independently without any significant interactions between the two binary components. In addition, they assumed that the stars in the binary were born from the same molecular cloud at approximately the same time.

This data set includes a chance alignment factor (R_{chance_align}) which determines the chance that the detected binary is in fact not a binary but two single stars that, due to chance, appear to be bound in a binary. This produces an upturn in the tail at larger separations. Section 3 of El-Badry et al. (2021) explains this in detail. We use this chance alignment factor and remove all binaries with $R_{chance_align} > 0.1$ which leaves us with 1389 binaries.

The apparent magnitudes of the WDs in the Gaia G-band, G , are limited to $13 \text{ mag} < G < 21 \text{ mag}$, however, this is not a cut done by the authors but a limitation on observational instruments. Using the parallax, p , we can estimate the absolute magnitude with

$$G_{abs} = G + 5 - 5 \log\left(\frac{1}{p}\right) \quad (1)$$

Using the parallaxes and apparent G-band magnitudes from Heintz et al. (2022) we estimate that the faintest WD in this data set will have an absolute magnitude in the G band of $\sim 16 \text{ mag}$. Thus we will remove all binaries where any member has a magnitude above this limit from our numerical data.

Figure 7 in Heintz et al. (2022) shows that in their dataset, for a large number of binaries, the cooling age of the primary, more massive, star is shorter than the secondary. This is not expected in isolated binaries and might indicate that these systems used to be triple systems where the inner binary interacted through mass transfer or a merger and later this inner binary was split or merged and thus formed a binary with the third object. These objects are removed from our comparisons.

3. Numerical simulations

3.1. The *mocca* code

We use the MOnte Carlo Cluster simulAtor, *mocca*¹, (Hypki & Giersz 2013; Giersz et al. 2013) and more specifically the simulations from MOCCA-SURVEY Database III which is an upgrade over the MOCCA-SURVEY Database II (Hypki et al. 2022) and MOCCA-SURVEY Database I (Askar et al. 2017). *mocca* is a GC simulator built on a Monte Carlo approach. It allows the usage of multiple stellar populations with different properties, large control over initial cluster conditions and allows quick evolution of large clusters with more than 1 million initial members.

An important aspect of the *mocca* code for our purposes is how stellar and binary evolution is treated, which is done with the modified *bse* code (Hurley et al. 2000, 2002). The *bse* code consists of a set of algorithms describing single star evolution, from zero-age main-sequence stars to later stages of stellar evolution, and binary evolution, taking into account angular momentum loss mechanisms, different modes of mass transfer, and tidal interaction. *bse* has been widely used to investigate different astrophysical objects and is characterized by its generally high level of accuracy in the analytic fitting formulae on which it is based.

Since the publication of *bse*, there have been several upgrades to the code (see, e.g. Kamlah et al. 2022, for more details). The main upgrades that are relevant for this study are the inclusion of a proper prescription for cataclysmic variable evolution (Belloni et al. 2018b, 2019) and the inclusion of improved wind prescriptions (Belczynski et al. 2016).

There are though two main problems in *bse* which play an important role on the types of binaries we are interested in. The first one is related to WD evolution, which is not properly handled by *bse*. The luminosity evolution of WDs is modelled in *bse* using the Mestel (1952) standard cooling theory. This theory though does not take into account important properties such as core composition and surface abundances as well as crucial features such as crystallization, which can significantly delay the WD cooling for Gyr and has been shown to be very important for explaining several features in WD populations (e.g. Tremblay et al. 2019; Schreiber et al. 2021; Bagnulo & Landstreet 2022; Blatman & Ginzburg 2024)

We therefore improved WD evolution in our analysis by computing more accurate WD properties via interpolation/extrapolation using the cooling sequences calculated by Bédard et al. (2020), assuming a thin hydrogen atmosphere. Provided the WD age and mass, we linearly interpolate/extrapolate through the sequences to obtain the WD properties such as effective temperature, radius and luminosity. These sequences were computed assuming solar metallicity, which is higher than assumed in our GC simulations. However, the impact of metallicity on WD evolution regarding the properties in which we are interested is virtually negligible (Renedo et al. 2010). That said, for the purposes of our analysis, it is reasonable to use the solar-metallicity sequences calculated by Bédard et al. (2020). The main motivation to use such sequences amongst the few that are available comes from the fact that they were used by Heintz et al. (2022).

3.2. Initial conditions

We use 197 cluster simulations with a wide range of initial cluster parameters. A full description of the different cluster initial conditions can be found in Hypki et al. (2024, in prep). The most important parameters are:

- We have many different combinations of sizes of clusters, from 550 thousand to 2.6 million initial objects (two multiple stellar populations).
- We have both tidally filling and underfilling clusters
- We have both 10% and 95% initial binary fraction
- We use a Kroupa mass function between 0.08 and 150 M_{\odot}
- Different Galactocentric distance
- Different properties of multiple populations

A big difference with these simulations compared to earlier simulations is that we are using multiple-stellar populations in the framework of asymptotic giant branch scenario (Calura et al. 2019) in these new simulations and thus a new path to GC evolution. Instead of having one tidally underfilling dense cluster we have two populations; one tidally filling (or slightly tidally underfilling), less dense population with a higher maximum initial stellar mass and one tidally underfilling, denser population. This leads to a large number of early escapers from the first population where approximately 30-40% of mass is removed in the first few Myr. These binaries are mostly primordial and undisturbed from dynamical interactions since they escape at an early stage before they have had time to interact with other objects. The second population is more dense but the maximum stellar mass is lower, there is no formation of massive stars in this population. This limit is set to 20 M_{\odot} which means that there are no supernovae forming BHs from the second population. The previously used initial cluster conditions are quite similar to the second population while the first population is not as tightly bound and is able to lose a lot of mass early in the evolution.

The choice of 10% or 95% binary fraction affects the initial binary properties. For example, in a 10% binary fraction cluster, the largest semi-major axis value is 100 au and the distribution is uniform in $\log(a)$. With 95% binary fraction, we allow binaries to form with larger separations and the initial distribution of semi-major axis and eccentricity is based on Kroupa (1995); Belloni et al. (2017). Since these binaries are often disrupted by dynamical interactions, a 95% binary fraction has been found to agree well with observations (Belloni et al. 2017, 2018a). For both binary fractions, the initial eccentricity distribution is thermal.

3.3. Star cluster and isolated binary evolution

For each initial setup, we ran two simulations; one with dynamical interactions between objects and one run with no dynamical interactions, i.e. pure binary/stellar evolution where all objects in our initial star cluster model are evolved in isolation. This allows us to understand the impact of dynamics on the primordial binary population and DWD formation. In addition, whenever an object is ejected from a cluster, we used *bse* to continue the evolution of this object. Furthermore, we split up primordial and dynamically formed binaries in the cluster simulation with dynamics. This gives the following 4 groups:

- Cluster-primordial: DWDs with progenitors born together found inside an evolving cluster.
- Cluster-dynamical: DWDs that were formed in a dynamical interaction found inside an evolving cluster.

¹ <http://moccacode.net>

- Standalone evolution: DWDs evolved in isolation
- Escapers: escaping DWDs from the cluster simulations. Evolved as isolated binaries after escape.

These simulations are run up to 15 Gyr in order for us to obtain data from a wide range of evolutionary stages at different times.

3.4. Further calculations

There is evidence for natal kicks on WDs (Davis et al. 2008; Hamers & Thompson 2019) that could lead to the destruction of fragile wide binaries. The magnitude of these kicks are believed to be on the order of ~ 0.75 km/s (El-Badry & Rix 2018). This is not included in our simulations and thus we apply the energy related to a kick of 0.75 km/s for each star to the binding energy of the binary. We check if this causes the binary to dissolve, if it does, we remove this binary from the sample. If not, we calculate the new semi-major axis related to the new binding energy. To calculate the absolute magnitude of the WDs from *molca* we use the *FSPS*² code (Conroy et al. 2009; Conroy & Gunn 2010). For one binary, this code can calculate the absolute magnitudes of both components in a binary using the mass, radius, luminosity and effective temperature. This provides us with absolute magnitudes for different instruments and filters, such as the Gaia G band.

3.5. Observational selection effects

Binary stars can be detected through different methods depending on the distance between the two components. Close binaries are detected through e.g. photometric surveys, spectroscopic observations or X-ray observations while wide binaries are too far apart to reliably use photometric data. Instead, if two wide separated stars have a common proper motion across the sky or similar radial velocities they can be classified as a binary candidate and in more detailed follow-up observations this can be confirmed. Due to the different methods of obtaining observational data, there are also different limitations. We need to consider these observational selection effects when comparing our data. Thus we apply different filtering criteria on the close and wide binaries respectively. These criteria are explained in the following sections.

3.5.1. Close binaries

For close binaries, we use the following filtering criteria on our *molca* data:

- $P < 1.5$ day
- $G < 11.24$ mag where G is the combined absolute magnitude of the two WDs:

$$G = -2.5 \log(10^{-0.4G_1} + 10^{-0.4G_2}) \quad (2)$$

where G_1 and G_2 is the absolute magnitudes in the G-band of the primary and secondary WD.

We did not use any filtering based on WD mass.

3.5.2. Wide binaries

For wide binaries, we use the following filtering criteria on our *molca* data:

- Semi-major axis: $a > 100$ AU
- Absolute magnitude: $G < 16.1$ mag
- Addition of kinetic energy corresponding to kicks of WDs to the binding energy of the binary (see Sect. 3.2).

As an additional step we use the total ages reported in Heintz et al. (2022), limited to $T_{age} < 10$ Gyr, and extract a subset of our data with the same age distribution. This gives us a data set with WDs with a wide range of ages. This filtering is only used for the results presented in Sect. 4.2.3.

3.6. Projection

It is often impossible to determine the semi-major axis of wide binaries from observational data. Instead, the projected separation between the two binary components is the parameter that can be determined. Due to this, to compare the binaries from our simulations to the observed binaries, we need to project our semi-major axis. The projection method we use is derived from chapter 2 of Hilditch (2001).

Assuming that we put one of the binary components at $(x, y, z) = (0, 0, 0)$. And assume that the xy plane is perpendicular to the line of sight of the observer, thus we cannot see the z -axis. We can calculate the projected position onto the x and y axes:

$$\begin{aligned} x &= r \cos \theta [\cos \Omega \cos \omega - \sin \Omega \sin \omega \cos i] + \\ &\quad r \sin \theta [-\cos \Omega \sin \omega - \sin \Omega \cos \omega \cos i] \\ y &= r \cos \theta [\sin \Omega \cos \omega + \cos \Omega \sin \omega \cos i] + \\ &\quad r \sin \theta [-\sin \Omega \sin \omega + \cos \Omega \cos \omega \cos i] \end{aligned} \quad (3)$$

where Ω is the longitude of the ascending node, ω is the longitude of periastron and i is the inclination of the orbit (see Fig. 2.5 in Hilditch (2001)). At pericenter and apocenter ($\theta = 0$ and $\theta = \pi$ respectively) We have $\sin(0) = \sin(\pi) = 0$:

$$\begin{aligned} x &= r \cos \theta [\cos \Omega \cos \omega - \sin \Omega \sin \omega \cos i] \\ y &= r \cos \theta [\sin \Omega \cos \omega + \cos \Omega \sin \omega \cos i] \end{aligned} \quad (4)$$

To get an average value of the projection fraction f_p , the average value that the semi-major axis is changed when projected onto the sky, we integrate over all angles; Ω from 0 to π , and ω & i from 0 to $\pi/2$. This gives

$$x = y \approx -0.2584 r \quad (5)$$

The projection fraction is thus

$$f_p = \sqrt{x^2 + y^2} = 0.842 \quad (6)$$

which is used to calculate the projected distance as:

$$a_{proj} = a \cdot f_p \quad (7)$$

where a is the semi-major axis of the binary.

4. Results

We start the presentation of our results by comparing the projected separation (calculated according to Sect. 3.6) with the mass of the WDs. For the observed close binaries we only consider the mass of the lower mass WD since the higher mass WD is typically not visible and the errors in the masses are usually very large. For all other data sets, both observations and simulations, we consider the mass of both WDs. Since observed

² <https://github.com/cconroy20/fspd>

close binaries cannot be resolved individually, there is no observational data for the separation of these binaries. Instead, we assume that the eccentricity of these binaries is 0 due to circularization and calculate the semi-major axis using Kepler's third law.

In Fig. 1 we show the projected separation plotted against the mass of the WDs for clusters with 10% and 95% respectively initial binary fraction at 9 Gyrs snapshot. This plot shows the whole range of separations, from close to wide, for the four different groups defined in Sec. 3.3.

Due to the many similarities and lack of clear differences in the overall picture for 10% and 95% binary fraction we will discuss both datasets together. We do not filter on magnitude in this section since the magnitude limits are different in different regions of the plot.

A noticeable feature of the in-cluster binaries is a gap in separations between 0.6 AU and 25 AU. This gap only exists for in-cluster binaries while for both escapers and isolated ones many systems are occupying this region in the parameter space. The reason for this gap is dynamics, more specifically, the threshold between soft and hard binaries lies in this gap. Binaries below this threshold will, on average, become harder due to dynamical interactions while binaries above will, on average, become softer as a result of dynamical interactions. This pushes binaries away from the threshold and creates this gap. This is one example of how important dynamical interactions can be for binaries in these dense environments.

The distribution of escapers is very similar to isolated binaries on a statistical scale. However, a very noticeable trend is that for all times and across all GC models we have far more escaped DWDs than isolated DWDs. The exact number depends on initial conditions and evolution time but we found that usually this ratio is between 1 and 3. This seems to indicate that dynamics play an important role in the formation of these binaries and without dynamics the formation of these binaries are not as effective as when dynamical interactions are included.

There is also a big difference in the number of escapers and in-cluster binaries. The reason for this is most likely due to stellar evolution leading to rapid mass loss from the evolution of massive stars in the first hundred Myr of the cluster evolution. When the stars are initially evolving and losing mass the tidal radius is decreased strongly and rapidly. This means that many binaries are suddenly outside of the tidal radius and thus counted as escapers. The binaries can later evolve into DWDs. We discuss this in more detail in Sect. 3.2.

For very low separations, there is a hook shaped formation, particularly for escapers and in-cluster binaries. This is related to cataclysmic variables that have later evolved into a DWD system. The fact that we have far fewer systems in this formation for isolated binaries once again shows the importance of dynamical interactions leading to their formation. For escapers in the 10% initial binary fraction datasets there are also a few lines going towards lower separations. These are also related to cataclysmic variables.

The observations of DWDs are currently limited to either spectroscopic binaries or wide binaries DWDs. While themocca data spans a wide range of separations and masses while observations are either for very close binaries or for very wide. We can clearly see that the observations are only including a very small part of the whole population. Because of this, we cannot do a direct comparison between mocca data and observations. We split our results into close and wide binaries and restrict our mocca data as explained in sections 3.5.1 and 3.5.2. The results

for close binaries are found in Sect. 4.1 and for wide binaries in Sect. 4.2.

4.1. Close binaries

In order to go into more detail when looking at the close binaries we isolate binaries according to the criteria described in 3.5.1 and will thus only focus on a small subset of the total population. We plot the projected separation against mass of the lower mass WD in Fig. 2 and 3. We only include the mass of the lower mass WD since, due to the observational technique, the errors in mass of the higher mass WD are often very large. Due to our limit on magnitude, we see that over time, higher mass WDs are not visible due to the cooling process of WDs. Already at 5 Gyr, all WDs with masses higher than $\sim 0.55M_{\odot}$ are now undetectable.

4.1.1. 10% initial binary fraction

We will start by looking at the 10% initial binary fraction plots in Fig. 2. At 2 Gyr the separations from all mocca datasets are slightly too wide and the masses too high. At 5 Gyr, escapers and isolated binaries agree very well with observations in separation. The in-cluster binaries at this time are biased towards lower separations than the other data-sets. At 9 Gyr, not much changes compared to 5 Gyr, the maximum mass is slightly lower due to more binaries being non-detectable due to increasing magnitude as they cool down. However, for all snapshots, the masses are not well reproduced. We are not able to produce very low mass WDs with mass below $0.2 M_{\odot}$ in our simulations. Instead, our close WDs usually have a mass between 0.25 and $0.4 M_{\odot}$. There are a few observed WDs in this mass range as well but the large majority is smaller mass.

These ELMs cannot form through common envelope evolution which produces a problem for our comparisons. Currently, bse does not handle this kind of evolution well. There is a large uncertainty in the magnetic braking, mass stability criteria and mass transfer modelling. More precisely, to form these objects we need dynamically stable mass transfer (e.g. Belloni & Schreiber 2023b). During this stable mass transfer involving a Roche-lobe filling subgiant or an unevolved red giant star, due to strong magnetic braking, the evolution is convergent and the binary evolves towards shorter orbital periods. This kind of mass transfer is not handled by bse or any other population synthesis code at this moment in time. In order to be able to properly reproduce the distribution of mass for these kinds of ELMs, upgrades to our bse are needed, however, that is outside of the scope of this paper.

Escaping binaries are able to form lower mass WDs than in-cluster or isolated binaries which can be seen as a sub-population between 0.3 and $0.45 M_{\odot}$. This is most likely due to dynamical interactions before they escaped their host cluster. The in-cluster binaries that would form these low mass WDs are either escaping or dynamical interactions are causing an exchange, a break-up or a merger.

At $\sim 0.51 M_{\odot}$ we can see a soft limit for WD masses. There are WDs with lower mass than this but they are few. This is a limit in bse and a lower mass would require processes that are neither in bse or solved in theory. This includes, as mentioned above, uncertainty in magnetic braking, mass stability criteria and mass transfer modelling.

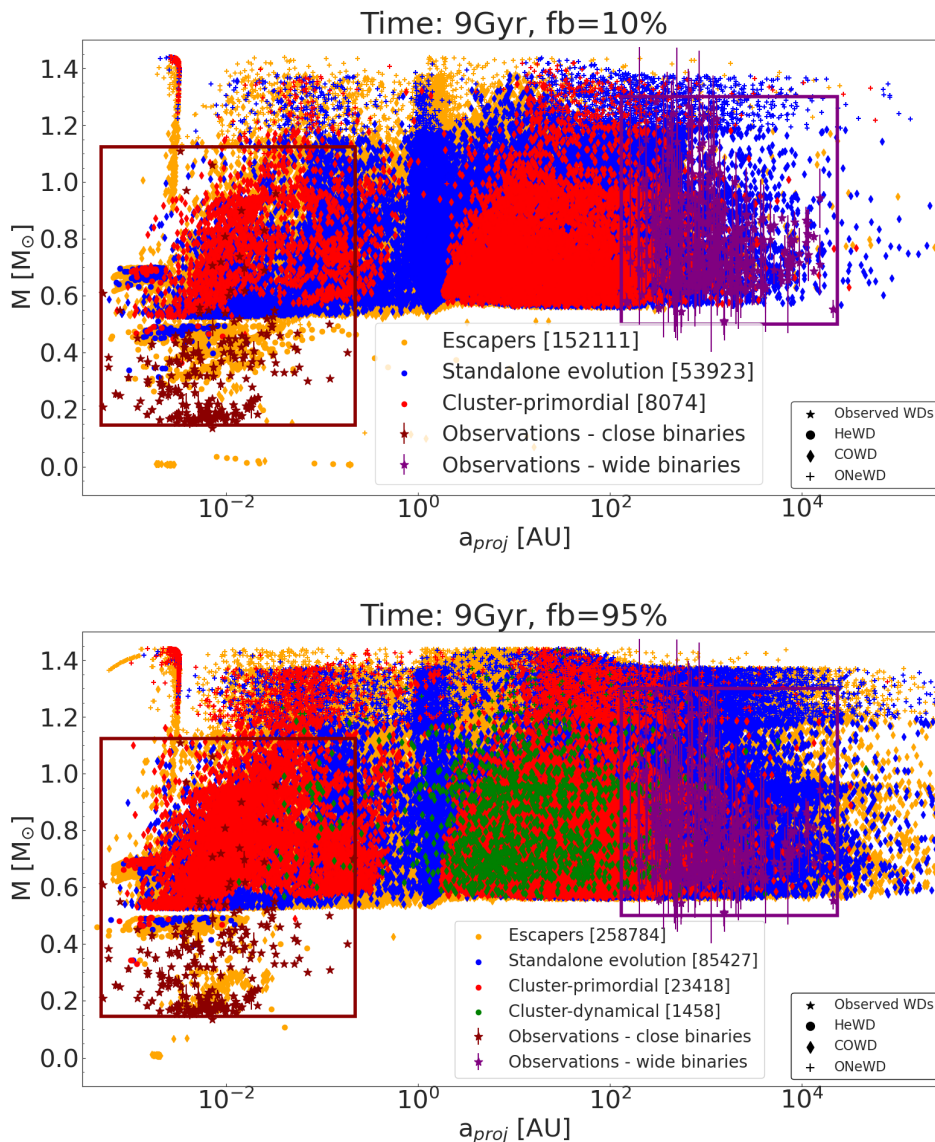


Fig. 1. Projected separation plotted against mass of the lower mass WD in the binary for 10% (panel a) and 95% (panel b) initial binary fraction for the whole parameter space. The numbers inside the square brackets in the legends show the total number of WD binaries in the runs. The different colours correspond to the different datasets: orange for escapers, blue for standalone binaries, red for in-cluster primordial binaries, green for in-cluster dynamically formed binaries, dark red for observations of close binaries and purple for observations of wide binaries. In addition to this, we have four different types of markers: stars for observed WDs, circles for helium WDs, diamonds for carbon oxygen WDs, pluses for oxygen neon WDs

4.1.2. 95% initial binary fraction

For 95% initial binary fraction (Fig. 3) we have a similar scenario but there are small differences. At 2 Gyr we have a larger shift towards higher separations compared to 10% binary fraction. As expected, similarly to 10% binary fraction, we are not able to form the ELMs WDs that have been observed. At 5 and 9 Gyr, we have good agreement in separation between escapers, isolated binaries and observations. In-cluster binaries are biased towards lower separations.

Looking at the number of close binaries we can see that the number of binaries is increasing with time for escapers and isolated binaries since over time more binaries are escaping their host cluster or the components of the binary are evolving into WDs. However, for in-cluster binaries, the number is decreas-

ing due to escaping binaries and dynamical interactions causing break-ups, mergers or exchanges.

An interesting feature is a triangular shaped gap in Fig. 3, panel (a). This gap occurs between 0.02 and 0.07 AU in projected separation and 0.8 and 1.1 M_{\odot} in mass. This gap is present for all datasets and the reason for it is currently unknown, although it is most likely related to the correlated distributions of the initial binary populations.

4.2. Wide binaries

In this section, we report our results involving wide binaries that have been obtained by filtering our mocca data according to 3.5.2. We split our results into clusters with initial binary fraction of 10% and 95%. As we discussed in Sect. 4.1, our limit

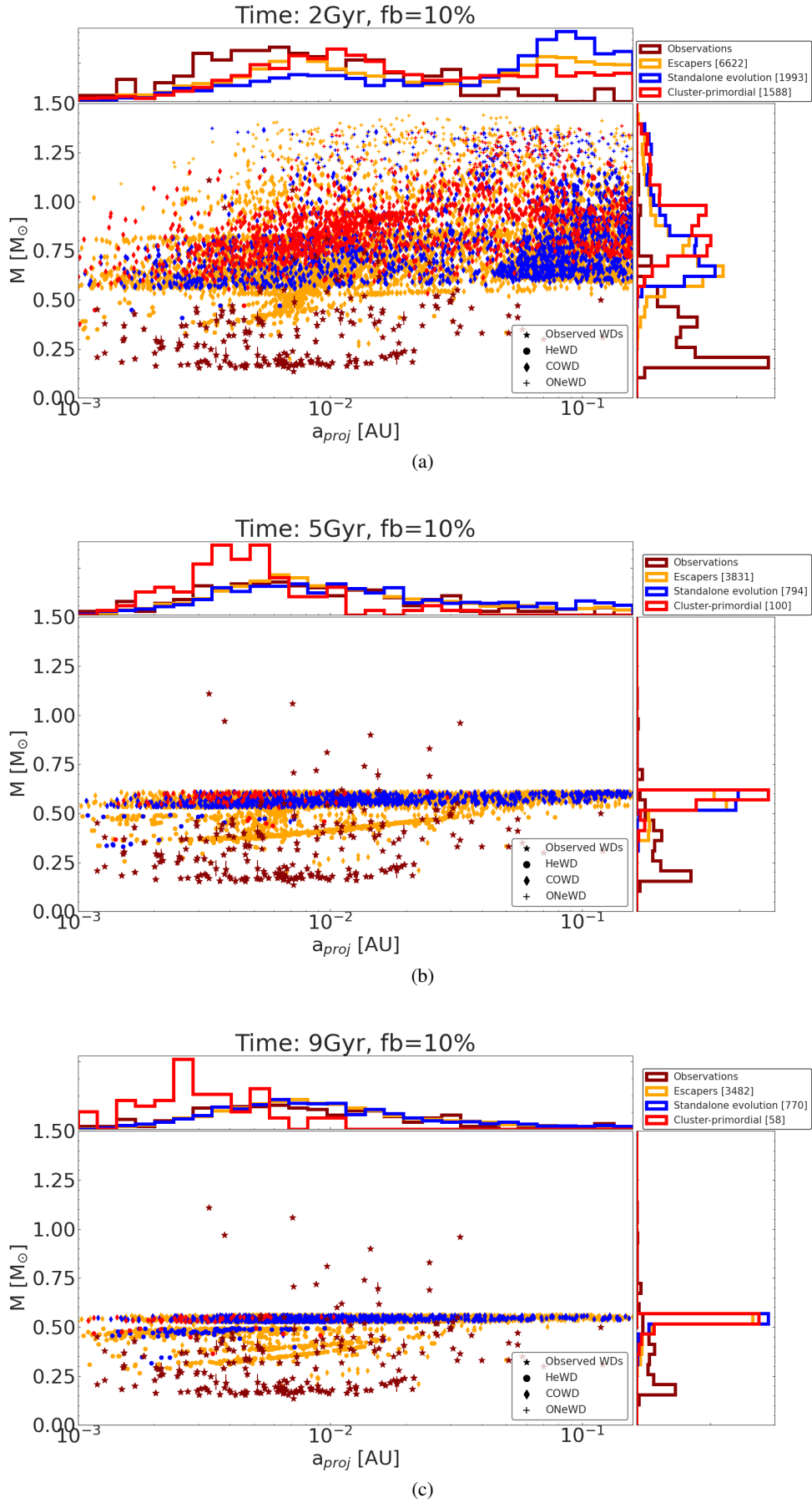


Fig. 2. Projected separation plotted against mass of the lower mass WD in the binary for close binaries inside clusters with 10% initial binary fraction. See Fig. 1 for an explanation of panels, markers and colours.

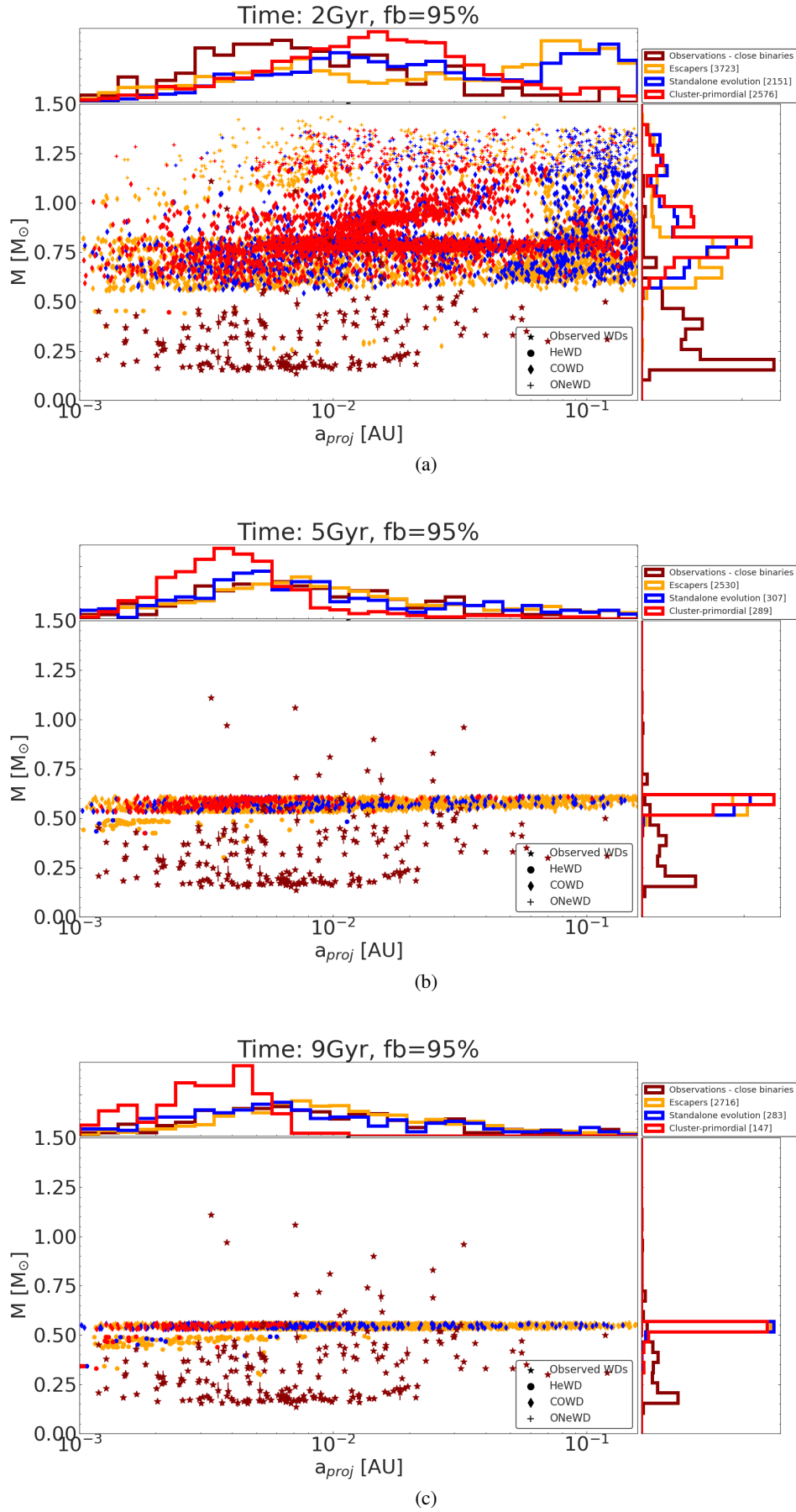


Fig. 3. Projected separation plotted against mass of the lower mass WD in the binary for close binaries inside clusters with 95% initial binary fraction. See Fig. 1 for an explanation of panels, colours and markers

in magnitude causes high mass WDs to become undetectable at later snapshots.

4.2.1. 10% Binary fraction

Figure 4 shows the distribution of projected separations plotted against mass of both binary components for 10% initial binary fraction at 2, 5 and 9 Gyr. For all snapshots, the binaries from mocca are not as wide as the observed binaries. This is because when we use 10% binary fraction, we have a cut-off at 100 au for initial semi-major axis. This is done under the assumption that the soft components of the binary populations are entirely gone and the remaining binaries are hard binaries. However, recent studies have shown that having nearly 100% initial binaries with most being soft is a better assumption. (e.g. Leigh et al. 2015; Belloni et al. 2019)

It is therefore unlikely that the binaries will evolve into larger separations. Since the absence of wide systems is seen in all three datasets, including the standalone evolution set, this cannot be due to dynamical interactions. Looking at the mass distribution we can see that the masses from our simulations, as expected, depend on time. Over time, lower mass WDs binaries are being formed as expected so for later times the distribution of masses gets lower, in addition to this, the cooling process causes high mass WDs to be undetectable at later times. We find that at 5 Gyr, our distribution aligns fairly well with the data from Heintz et al. (2022). At 2 Gyr the masses are biased towards higher masses while for 9 Gyr they are biased towards lower masses due to the cooling of WDs.

4.2.2. 95% binary fraction

When using 95% binary fraction we allow wider binaries to be formed initially. This causes our separation distribution to be more shifted towards wider binaries. This is shown in Fig. 5. All 3 datasets from mocca are very similar for all snapshots but we will point out the small differences. At 2 Gyr we have a tail extending towards wider binaries but our distribution is still biased towards lower separations than the observations. The masses do not align very well at this snapshot, they are too high and the observed WDs have noticeably lower masses. Escapers and isolated binaries are very similar in their separation distribution while in-cluster binaries have slightly lower separations which could be due to disruptions in dynamical interactions.

At 5 Gyr the separation distribution is very similar to the 2 Gyr snapshot. However, the masses agree much better with observations. Due to more time passing, lower mass WDs can form. In addition, the cooling sequence removes high mass WDs from our sample. This causes a good agreement with observations in mass. At 9 Gyr, the separation distribution does not change in any significant way. However, the cooling process has now made the higher mass WDs undetectable and we are left with a small subset of WDs with mass around $0.6 M_{\odot}$.

Similarly to the close binaries, we can see that over time the number of binaries increases in the escapers and standalone evolution datasets while decreasing in the cluster dataset.

4.2.3. Heintz age distribution

We can see in the previous plots that there is a time dependence in the mass distribution, both due to lower mass WDs being formed and higher mass WDs not being detectable due to the cooling process. This plot shows a sample of our DWDs with

the same age distribution as in Heintz et al. (2022). This is explained in Sect. 3.5.2. We can see that by doing this we indeed get a fairly good mass distribution, our masses are only slightly smaller but there is a bias and a peak at around $0.9 M_{\odot}$. This peak is connected to bse and in more detail to the envelope type. bse handles both convective and radiative envelopes but, as seen in this figure, the switch between may be too abrupt to be realistic. Nevertheless, if we would disregard this peak, our mass distribution agrees very well with observations.

However, this does not solve the problem of too low separations. This is most likely due to observational bias and WD binaries with lower separations are not observed or included in this observational survey. While the observations have a slight bell curve shape with a peak around 800 au, the mocca data extends to much lower separations and we are only looking at the far end tail. Due to this, we add an additional cut and only include binaries with projected separation above 500 au. This can be seen in Fig. 7 where our agreement between separation is much better. With these filtering procedures we can reproduce the observations in a very good way, in both projected separation and mass for all 3 of our simulated datasets.

5. Summary & Conclusions

In this paper, we have taken a large number of DWDs from a large number of mocca simulations and compared them to observed DWDs. This proved to be difficult due to strong observational biases. However, with some filtering and cuts on the mocca data, we managed to get good agreement in separation for close binaries and for both separation and masses for wide binaries. One important point about our data that should not be forgotten is that we are incorporating multiple stellar populations in our initial model. In these models, we have a first population that is tidally filling and not too concentrated and a second population that is significantly more concentrated than the first population. Thus our initial setup differs greatly from the traditional approach of having one dense initial population. In these new setups, we find a much larger number of escapers compared to simulations using the traditional one-population setup. We saw that many clusters lose 30-40% of their mass in just the first few Myr due to objects escaping the cluster induced by stellar evolution mass loss. Due to the early escape of these objects they are also mostly (or in many cases, completely) unaffected by dynamics before their escape. We can see this by the similarities in results between the 'standalone evolution' and 'escapers' data sets. This means that DWDs born in the field and those born inside GCs are, on average, similar.

Our GC initial conditions give us both tidally filling and underfilling clusters. Since tidally filling clusters will lose more mass in the early stages of the evolution, the number of escaping DWDs is expected to be different for these two different types as well. We find that from tidally filling clusters, there are approximately 2 times more DWD escapers at 2 Gyr and approximately 1.6 times more DWD escapers at 9 Gyr compared to tidally underfilling clusters. However, we do not find any significant differences in the statistical distribution of separations of DWDs that have escaped from tidally filling and underfilling clusters.

A significant finding is related to the number of DWDs in each set; we found that for most clusters and snapshots, the number of DWDs in the escaping dataset is far larger than the other two sets (in-cluster and standalone binaries). This is clearly shown in figure 8 where we plot the ratio between the number of escaping DWDs and standalone DWDs. For 95% binary fraction, we have slightly more escaping DWDs at 1 Gyr than stan-

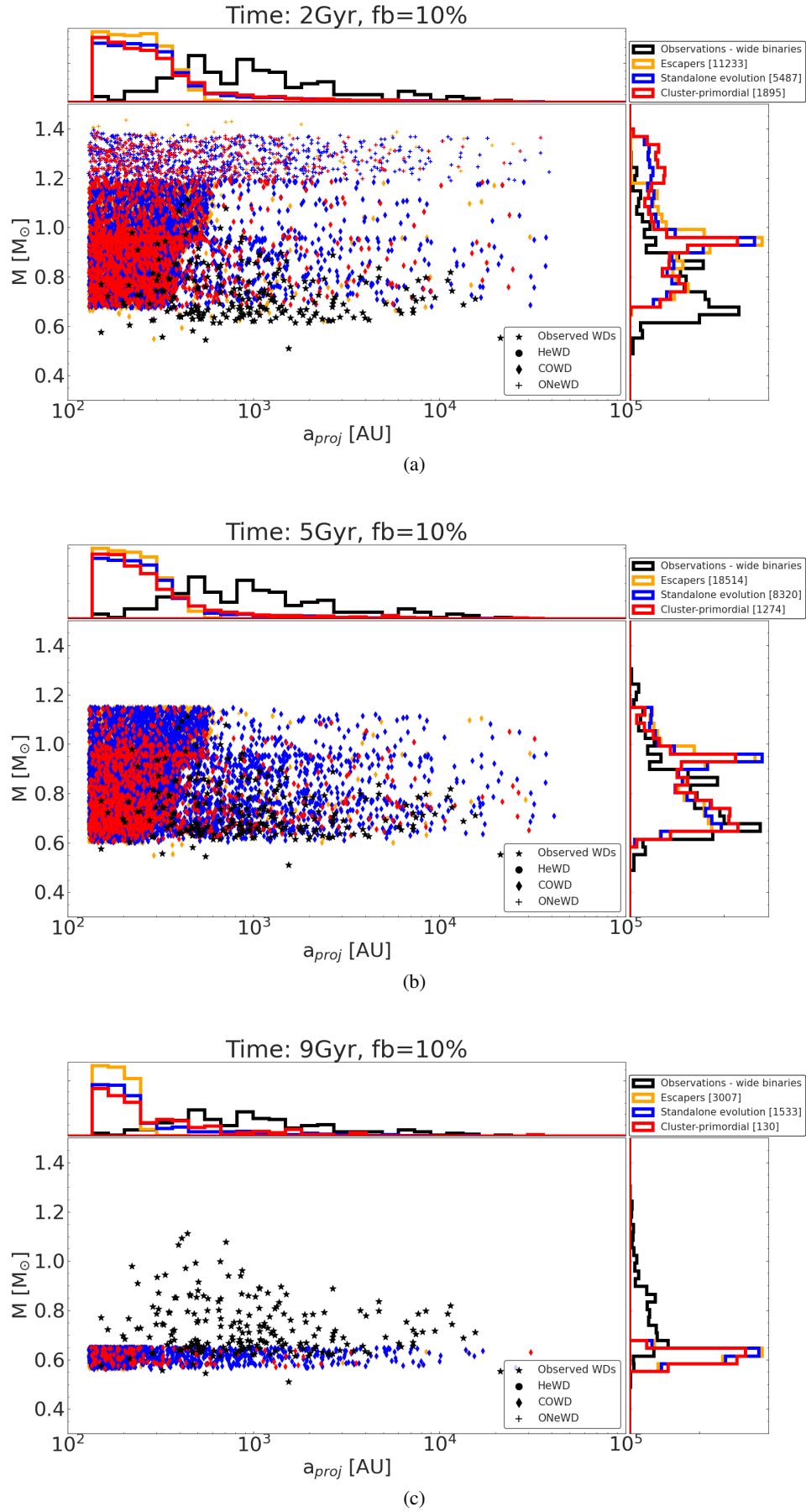


Fig. 4. Projected separation plotted against mass for wide binaries with 10% initial binary fraction. See Fig. 1 for an explanation of panels, colours and markers.

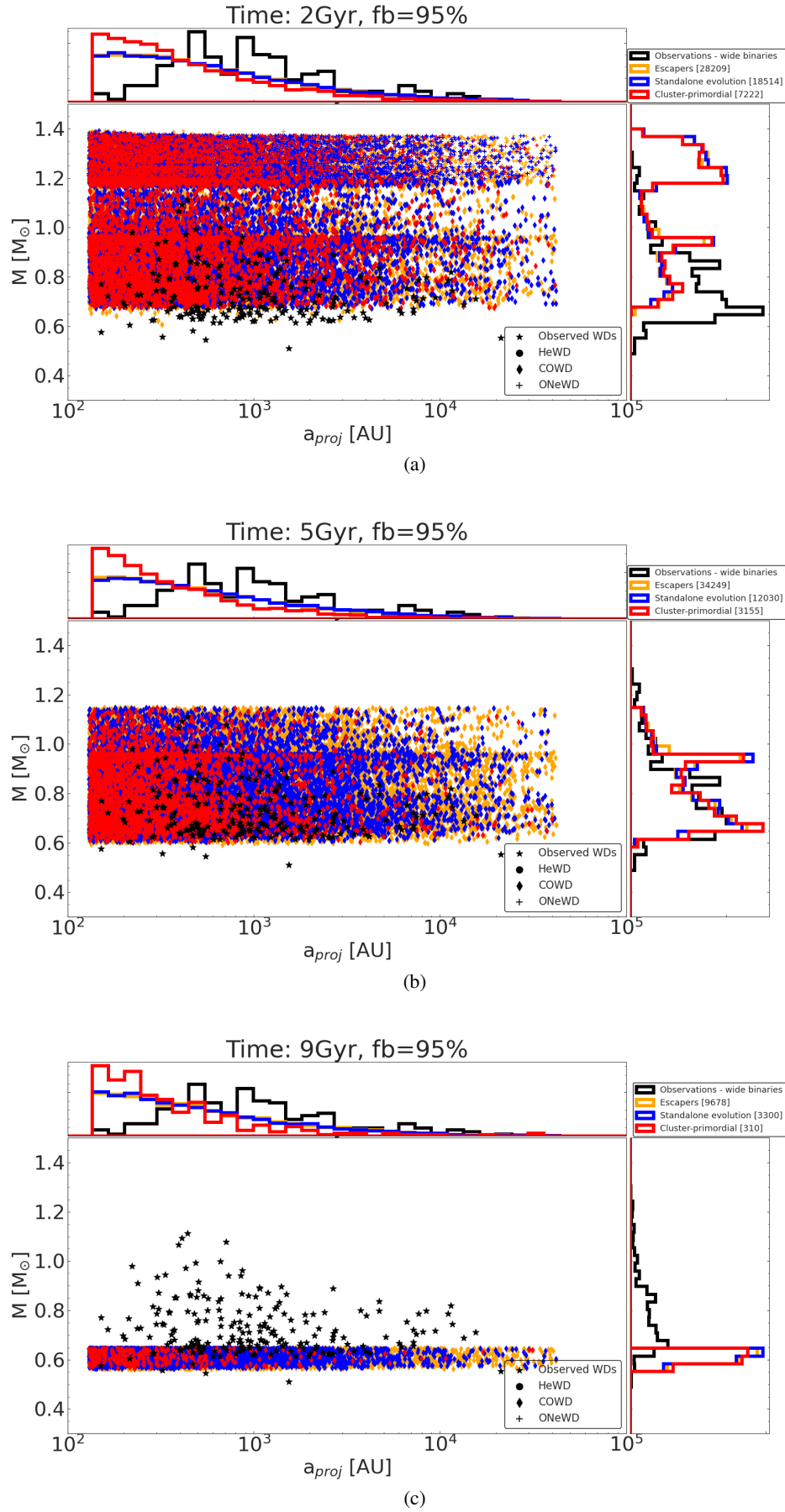


Fig. 5. Projected separation plotted against mass for wide binaries with 95% initial binary fraction. See Fig. 1 for an explanation of panels, colours and markers.

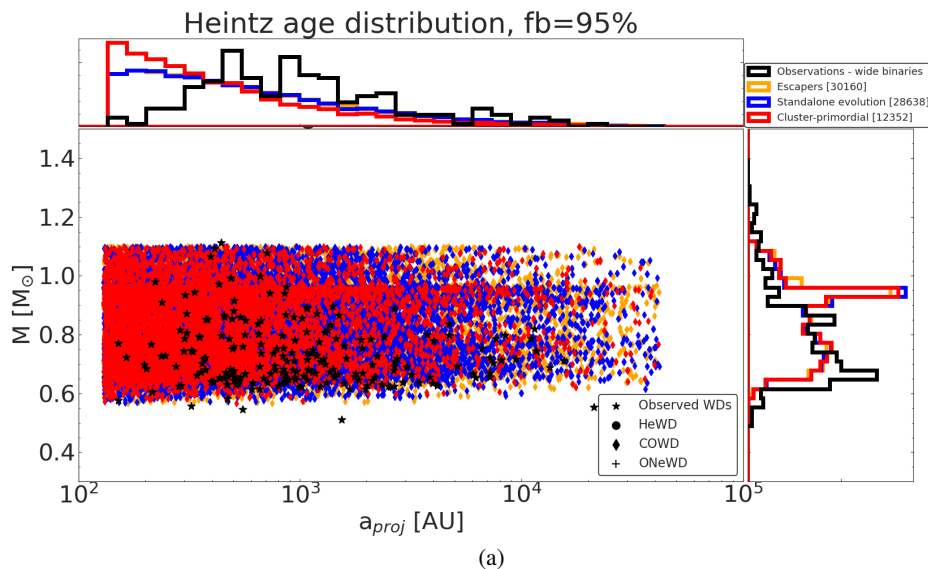


Fig. 6. Projected semi-major axis plotted against mass of the WDs for our set with an age distribution similar to Heintz et al. (2022). Panel (a) for 10% and (b) for 95%. See Fig. 1 for an explanation of colours and markers.

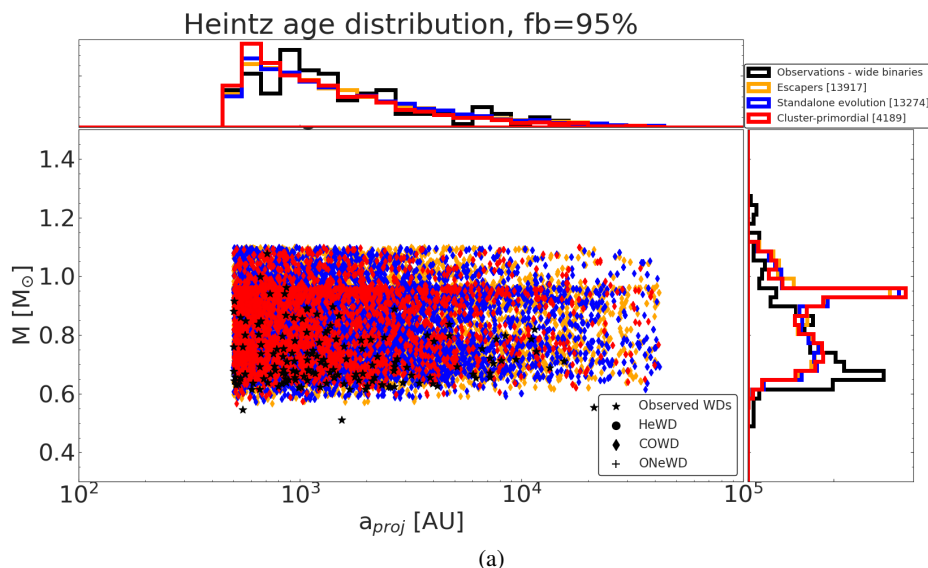


Fig. 7. Projected separation plotted against mass of the WDs in the binary. In this figure we added an additional cut-off at 500 au to remove the tail of lower separation binaries found in the observational data. We see good agreement in both mass and separation. See Fig. 1 for an explanation of colours and markers.

alone DWDs, however, at later times this ratio grows and we see a faster increase in the number of escaping DWDs. At 12 Gyr, we have approximately 3 times more escaping DWDs than standalone ones. For 10% binary fraction, we start with significantly less escaping DWDs. At 3 Gyr, we have approximately the same number and at later times we have more escaping than standalone. At 12 Gyr, we have almost 4 times more escaping DWDs than standalone. This indicates that even though many binaries escape early, they are still influenced by dynamics in a way that causes them to be more likely to form WDs within a Hubble time. This is true even for less dense clusters and clusters with a low binary fraction. For populations 1 and 2 separately, we can see that the big difference in this ratio comes from population 1, especially for 95% binary fraction at early times.

When looking at the whole range of semi-major axis (see Fig. 1 and ??) we can see a gap in the in-cluster population between ~ 0.5 and ~ 25 au. For the escape and standalone populations, we do not see this clear gap. This can be seen more clearly in Fig. 9 where we plot a histogram of the distribution of semi-major axis for the three data sets from mocca at 2 Gyr (panel a) and 9 Gyr (panel b) for 95% binary fraction. We also split populations 1 and 2 into separate groups in order to see the effect of the two populations. In the plot we clearly see the gap in the in-cluster set for both population 1 (dark-red) and population 2 (orange) at both times. Comparing the two populations at 2 Gyr, for small separations we have approximately 55% higher fraction of population 2 binaries than population 1 binaries. However, at larger separations, we have approximately 25% higher fraction of population 1 binaries than population 2 binaries. At 9

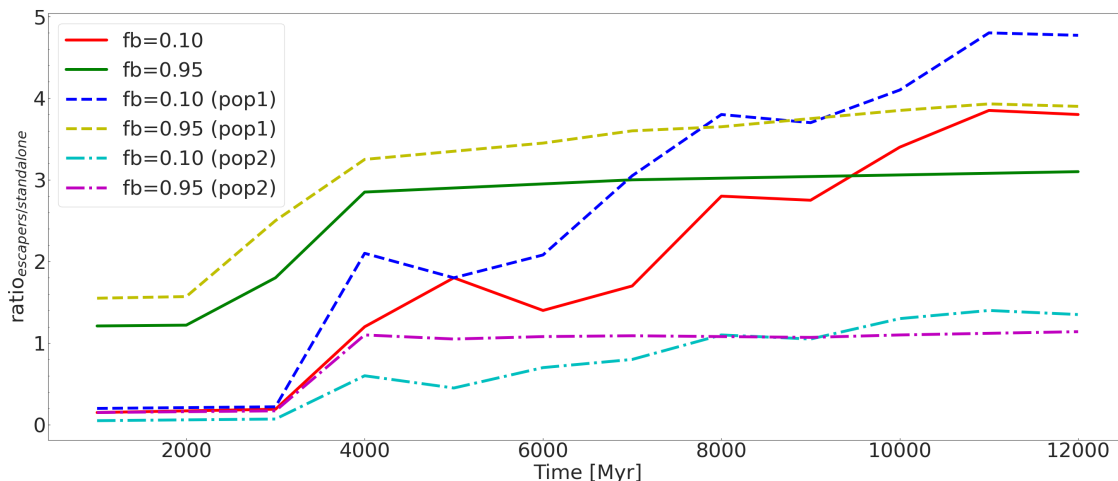


Fig. 8. Evolution of ratio between number of escaping DWDs and standalone DWDs for every Gyr between 1 and 12 Gyr. We have 6 groups in this figure; solid lines show both populations together, dashed lines show population 1 only and dotted lines show population 2 only.

Gyr the two populations have evened out and the differences are much smaller.

This gap is non-existent for the escapers and standalone data sets. Instead, there is a sharp increase by ~ 1 au. This big peak is mostly visible for escapers at 2 Gyr but is there for both data sets at both snapshots. This very big population of escaping binaries at ~ 1 AU seems to indicate that this gap is partly due to escaping binaries, however, the reason for these particular binaries to escape is still uncertain. The fact that we do see a similar peak, however, not as large, for the standalone runs seems to indicate that we have some bias in our initial datasets to create WD binaries with these separations. Combining this with a large mass loss in the first few Myr can lead to features like this. However, this paper aimed to compare our results to observations and finding a more conclusive answer to this gap is beyond the scope of this paper. We can also note that, from these plots, there are no significant differences in populations 1 and 2 for the escapers and standalone sets. Even though there is no statistical difference in the distribution of separation between populations 1 and 2, there is a clear number difference. We have almost 100 times more escapers from population 1 than 2, at both 2 and 9 Gyr. This causes population 1 to provide the large bulk of escaping binaries when analysing the data as a whole.

Our main conclusions can be summarised as:

- Observations of DWD systems are biased and limited which make direct comparisons impossible without filtering mocca data.
- When using a 10% binary fraction, we are not able to reproduce the separation distribution of wide binaries. This is due to how the initial distribution of semi-major axis is setup for a 10% initial binary fraction cluster (see Fig. 4).
- Using 95% binary fraction with initial semi-major axis distribution given by Belloni et al. (2017) allows us to form wider binaries that agree better with observations (see Fig. 5)
- Using a similar age distribution as in Heintz et al. (2022) and adding a lower limit to the separation causes our 95% binary fraction dataset to agree very well with observations in both separation and masses (see Fig. 7)
- The masses of WDs in wide binaries agree well with observations at 5 Gyr, but are too high at 2 Gyr and too low at 9 Gyr. This is true for both 10% and 95% binary fraction.

- For close binaries, our data agrees well with observed binaries in separation. In particular for escapers and isolated binaries but the in-cluster binaries also agree fairly well (see Fig. 2 and 3).
- The very low masses of ELM WDs are not able to be reproduced with bse. Uncertainties in binary evolution related to magnetic braking, mass stability criteria and mass transfer modelling makes it impossible to form these extremely low mass WDs.
- Due to the addition of multi-stellar populations and a less dense first population, a large amount of objects are removed from the clusters in the first few Myr. This leads to a much larger number of escapers than in-cluster binaries and standalone evolution binaries. The main difference between the escapers and standalone binaries is that the escapers have the possibility to be hardened in dynamical interactions before their escape. This can cause wide binaries to form DWDs on a shorter timescale, thus increasing the number of escaping DWDs.
- The cooling sequence of WDs and the magnitude limits of observations indicate the mostly young WDs are being observed. This is confirmed by the age estimates from Heintz et al. (2022) where a majority of binaries have an age less than 3 Gyr.
- There is room for future analysis on these subjects, in particular the gap that we found in the separations of DWDs. The focus on this paper was on comparisons to observations and we were not able to find a concrete explanation to this gap. Also, with future observational missions there will be more data available. This would lead to better comparisons to simulated data, especially since most observational data is constrained to either close or wide binaries.

Acknowledgments

LH, GM, AH, AA, GW were supported by the Polish National Science Center (NCN) through the grant UMO-2016/23/B/ST9/02732. DB acknowledges financial support from FONDECYT grant number 3220167.

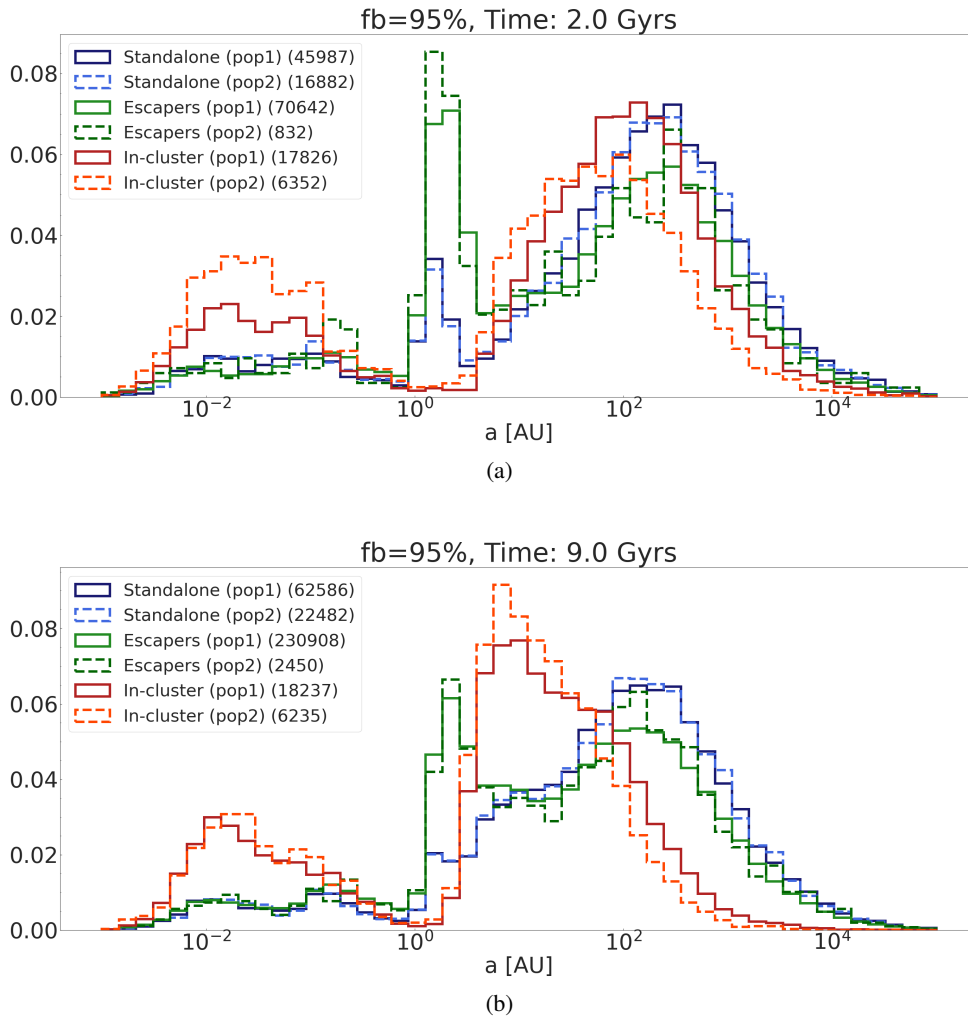


Fig. 9. Histogram of the semi-major axis distribution for the three mocca datasets with population 1 and 2 split into different groups from a snapshot at 9 Gyr for 95% binary fraction.

Data Availability

Input and output data for the globular cluster simulations carried out in this paper will be shared on request to the corresponding author.³

References

- Amaro-Seoane, P., Andrews, J., Arca Sedda, M., et al. 2023, *Living Reviews in Relativity*, 26, 2
- Arca Sedda, M., Kamlah, A. W. H., Spurzem, R., et al. 2024, *MNRAS*, 528, 5119
- Askar, A., Szkudlarek, M., Gondek-Rosińska, D., Giersz, M., & Bulik, T. 2017, *MNRAS*, 464, L36
- Bagnulo, S. & Landstreet, J. D. 2022, *ApJ*, 935, L12
- Banerjee, S. 2022, *A&A*, 665, A20
- Bastian, N. & Lardo, C. 2018, *ARA&A*, 56, 83
- Bédard, A., Bergeron, P., Brassard, P., & Fontaine, G. 2020, *ApJ*, 901, 93
- Bédard, A., Blouin, S., & Cheng, S. 2024, *Nature*, 627, 286
- Belczynski, K., Heger, A., Gladysz, W., et al. 2016, *A&A*, 594, A97
- Belloni, D., Askar, A., Giersz, M., Kroupa, P., & Rocha-Pinto, H. J. 2017, *MNRAS*, 471, 2812
- Belloni, D., Giersz, M., Rivera Sandoval, L. E., Askar, A., & Cielieć, P. 2019, *MNRAS*, 483, 315
- Belloni, D., Kroupa, P., Rocha-Pinto, H. J., & Giersz, M. 2018a, *MNRAS*, 474, 3740
- Belloni, D. & Schreiber, M. R. 2023a, in *Handbook of X-ray and Gamma-ray Astrophysics*. Edited by Cosimo Bambi and Andrea Santangelo, 129
- Belloni, D. & Schreiber, M. R. 2023b, *A&A*, 678, A34
- Belloni, D., Schreiber, M. R., Zorotovic, M., et al. 2018b, *MNRAS*, 478, 5626
- Blatman, D. & Ginzburg, S. 2024, *MNRAS*, 528, 3153
- Brown, W. R., Kilic, M., Kosakowski, A., et al. 2020, *ApJ*, 889, 49
- Calura, F., D’Ercole, A., Vesperini, E., Vanzella, E., & Sollima, A. 2019, *MNRAS*, 489, 3269
- Campos, F., Pelisoli, I., Kamann, S., et al. 2018, *MNRAS*, 481, 4397
- Carvalho, G. A., dos Anjos, R. C., Coelho, J. G., et al. 2022, *The Astrophysical Journal*, 940, 90
- Conroy, C. & Gunn, J. E. 2010, *ApJ*, 712, 833
- Conroy, C., Gunn, J. E., & White, M. 2009, *ApJ*, 699, 486
- Davis, D. S., Richer, H. B., King, I. R., et al. 2008, *Monthly Notices of the Royal Astronomical Society: Letters*, 383, L20
- Drewes, M., McDonald, J., Sablon, L., & Vitagliano, E. 2022, *The Astrophysical Journal*, 934, 99
- El-Badry, K. & Rix, H.-W. 2018, *MNRAS*, 480, 4884
- El-Badry, K., Rix, H.-W., & Heintz, T. M. 2021, *MNRAS*, 506, 2269
- Fontaine, G., Brassard, P., & Bergeron, P. 2001, *PASP*, 113, 409
- Gaia Collaboration, Brown, A. G. A., Vallenari, A., et al. 2021, *A&A*, 649, A1
- Giersz, M., Heggie, D. C., Hurley, J. R., & Hypki, A. 2013, *MNRAS*, 431, 2184
- Gratton, R. G., Carretta, E., & Bragaglia, A. 2012, *A&A Rev.*, 20, 50
- Hamers, A. S. & Thompson, T. A. 2019, *The Astrophysical Journal*, 882, 24
- Heintz, T. M., Hermes, J. J., El-Badry, K., et al. 2022, *ApJ*, 934, 148
- Hilditch, R. W. 2001, *An Introduction to Close Binary Stars* (Cambridge University Press)
- Hurley, J. R., Pols, O. R., & Tout, C. A. 2000, *MNRAS*, 315, 543
- Hurley, J. R., Tout, C. A., & Pols, O. R. 2002, *MNRAS*, 329, 897
- Hypki, A. & Giersz, M. 2013, *MNRAS*, 429, 1221

³ <https://zenodo.org/records/10865904>

- Hypki, A., Giersz, M., Hong, J., et al. 2022, *MNRAS*, 517, 4768
Kamlah, A. W. H., Leveque, A., Spurzem, R., et al. 2022, *MNRAS*, 511, 4060
Kosakowski, A., Brown, W. R., Kilic, M., et al. 2023, *ApJ*, 950, 141
Kratler, K. M. 2011, *The Formation of Binaries*
Kremer, K., Rui, N. Z., Weatherford, N. C., et al. 2021, *ApJ*, 917, 28
Kremer, K., Ye, C. S., Rui, N. Z., et al. 2020, *ApJS*, 247, 48
Kroupa, P. 1995, *MNRAS*, 277, 1507
Lee, Y.-W., Joo, J.-M., Sohn, Y.-J., et al. 1999, *Nature*, 402, 55
Leigh, N. W. C., Giersz, M., Marks, M., et al. 2015, *MNRAS*, 446, 226
Liu, J. 2009, *Monthly Notices of the Royal Astronomical Society*, 400, 1850
Maselli, A., Marassi, S., & Branchesi, M. 2020, *A&A*, 635, A120
Mestel, L. 1952, *MNRAS*, 112, 583
Renedo, I., Althaus, L. G., Miller Bertolami, M. M., et al. 2010, *ApJ*, 717, 183
Rodriguez, C. L., Coughlin, S. C., Weatherford, N. C., et al. 2021, *ClusterMonteCarlo/CMC-COSMIC: Release Version of CMC*
Schreiber, M. R., Belloni, D., Gänsicke, B. T., Parsons, S. G., & Zorotovic, M. 2021, *Nature Astronomy*, 5, 648
Schreiber, M. R., Belloni, D., Zorotovic, M., et al. 2022, *MNRAS*, 513, 3090
Torres, S., García-Berro, E., Althaus, L. G., & Camisassa, M. E. 2015, *A&A*, 581, A90
Tremblay, P.-E., Fontaine, G., Gentile Fusillo, N. P., et al. 2019, *Nature*, 565, 202
Wang, L., Iwasawa, M., Nitadori, K., & Makino, J. 2020, *MNRAS*, 497, 536
Wang, L., Spurzem, R., Aarseth, S., et al. 2016, *MNRAS*, 458, 1450
Wang, L., Spurzem, R., Aarseth, S., et al. 2015, *MNRAS*, 450, 4070